Lung muscarinic receptor occupancy by tiotropium: translational PET studies in non-human primates and humans

Zsolt Cselényi (zsolt.cselenyi@astrazeneca.com)
AstraZeneca Sweden: AstraZeneca AB https://orcid.org/0000-0002-8479-6282

Aurelija Jucaite
AstraZeneca Sweden: AstraZeneca AB

Pär Ewing
AstraZeneca Sweden: AstraZeneca AB

Per Stenkrona
Karolinska Institutet Institutionen for klinisk neurovetenskap

Cecilia Kristensson
AstraZeneca Sweden: AstraZeneca AB

Peter Johnström
AstraZeneca Sweden: AstraZeneca AB

Magnus Schou
AstraZeneca Sweden: AstraZeneca AB

Martin Bolin
Karolinska Institutet Institutionen for klinisk neurovetenskap

Christer Halldin
Karolinska Institutet Institutionen for klinisk neurovetenskap

Bengt Larsson
AstraZeneca Sweden: AstraZeneca AB

Ken Grime
AstraZeneca Sweden: AstraZeneca AB

Ulf G Eriksson
AstraZeneca Sweden: AstraZeneca AB

Lars Farde
Karolinska Institutet Institutionen for klinisk neurovetenskap

Research Article

Keywords: Positron emission tomography, [11C]VC-002, muscarinic receptors, receptor occupancy, lungs, tiotropium

Posted Date: February 24th, 2022

DOI: https://doi.org/10.21203/rs.3.rs-1336103/v1

Abstract

Background

The aim of the present translational PET study was to estimate occupancy of tiotropium at muscarinic acetylcholine receptors (mAChR) in the lungs *in vivo*.

The relationship between the tiotropium exposure and receptor occupancy (RO) in the lung was assessed in non-human primates (NHPs) after intravenous injection of tiotropium doses at a broad dose interval (0.1-1mg/kg). The feasibility of measuring mAChR occupancy in the human lung was then confirmed in seven healthy human subjects after inhalation of a single therapeutic dose of tiotropium (18mg). PET examinations were performed using radioligand [^{11}C]VC-002. Occupancy in lungs was estimated using Lassen plot analysis of parametric images showing total radioligand binding (total distribution volume, V_T).

Results

There was an evident effect of tiotropium on [^{11}C]VC-002 binding to mAChRs in lungs in both NHPs and humans. In NHPs, the occupancy was 11 to 78%, increasing in a dose dependent manner. The Lassen-plot based estimate of non-displaceable binding in NHPs was about 10% of the V_T. In humans, occupancy was 6-65%, and non-displaceable binding (V_{ND}) was about 20% of total binding, V_T at baseline.

Conclusions

The results demonstrated that [^{11}C]VC-002 binds specifically to mAChRs in the lungs such that it allows for the detection and quantification of lung muscarinic receptor occupancy following administration of an intravenously administered or inhaled muscarinic antagonist drugs. The methodology has potential for dose finding and comparison of drug formulations in future applied studies.

Clinical Trial Registration: ClinicalTrials.gov identifier: NCT03097380, registered: 31 March 2017, url: https://clinicaltrials.gov/ct2/show/NCT03097380

Background

Muscarinic receptor (mAChR) antagonists together with other bronchodilators are the current mainstay for relieving dyspnoea in patients with chronic lung disorders (Matera et al 2020; Maia et al 2017, Melani 2015). The clinical efficacy of the first long-acting mAChR antagonist (LAMA) tiotropium has over the years spurred development of new LAMAs (Lal et al 2020). However, despite their widespread use, the extent and duration of LAMA binding to receptors in human lung tissue *in vivo* is still poorly understood (Backman et al 2014).

Receptor occupancy refers to the percentage of a receptor population that is occupied by a drug targeting the receptors at a specified dose or concentration in plasma. The concept of receptor occupancy (RO) was

early introduced in positron emission tomography (PET) studies of drugs used to treat neuropsychiatric disorders (Farde et al 1988, Waarde et al 2000). It serves as a correlate of pharmacodynamic and safety parameters, thereby supporting selection of optimal dose strength and dosing interval to be examined in clinical trials (Lee and Farde, 2006, Varnäs et al 2011, Nord et al, 2011, Jucaite et al 2013, 2017).

Using the radioligand [^{11}C]VC-002 we recently performed a PET study in nonhuman primates (NHP), with the aim to determine and compare lung mAChR occupancy after inhalation and iv infusion of the LAMA ipratropium (Shou et al 2019). The study showed that it is possible to demonstrate a dose-occupancy relationship in lung and demonstrated the therapeutic advantage of the inhaled route of drug delivery. [^{11}C]VC-002 binding to muscarinic receptors has very recently been further examined in a test-retest study in humans (Cselényi et al 2020). It was concluded that the kinetic behaviour and the binding characteristics of the radioligand appears suitable for applied studies on muscarinic receptor occupancy in the human lungs.

The aim of the present translational PET study was to estimate occupancy of tiotropium at mAChR in the lungs *in vivo*. The relationship between the tiotropium exposure and receptor occupancy was assessed in NHPs after intravenous injection of doses covering a broad range. The feasibility of measuring mAChR occupancy was then confirmed in a small sample of healthy human subjects after inhalation of a single therapeutic dose of tiotropium.

Subjects And Methods

Study in non-human primates

The study was approved by the Animal Research Ethical Committee of the Northern Stockholm Region. Three adult female cynomolgus monkeys (mean weight 6.1 kg) were included. The non-human primates (NHPs) were owned by the Centre for Psychiatry Research, Department of Clinical Neuroscience, Karolinska Institutet, and housed in the Astrid Fagraeus Laboratory, Karolinska Institutet,, Solna, Sweden.

Study design

The study in NHP comprised of 8 experimental days. Two PET-measurements with [^{11}C]VC-002 were performed on each day. A baseline PET-measurement was followed by a second measurement 2.5h later either at baseline conditions (test-retest) or after i.v. administration of tiotropium (pretreatment). Two of the monkeys (NHP1 and NHP2) participated in the test-retest measurements. All three monkeys (NHP1-3) participated in two pretreatment sessions each. In the pretreatment measurements (n = 6), tiotropium was infused over 15 min starting 20 min before the [^{11}C]VC-002 injection (for details see supplement figure S1). The six doses of tiotropium varied from 0.03 to 1.0 µg/kg. The highest doses were expected to induce saturating levels of tiotropium binding in lungs. In contrast to humans, such conditions were feasible as higher doses were well tolerated in NHP.

Measurement of tiotropium plasma concentration

At each PET measurement with active drug, venous blood samples were collected for determination of tiotropium plasma concentration. The samples were drawn before tiotropium administration at approximately 35 min before [^{11}C]VC-002 injection, and after tiotropium administration at 0.5, 1, 5, 15, 30 and 60 min after [^{11}C]VC-002 injection. The plasma concentration of tiotropium was measured by solid phase extraction, followed by high-performance liquid chromatography and atmospheric pressure chemical ionization tandem mass spectrometry (Hohlfeld et al 2014). The lower limit of quantification (LLOQ) was 5 pM. The area under the plasma concentration curve for the time of the PET measurement (90 min) was calculated and divided by the duration to obtain the average plasma concentration during PET.

PET measurements

General anaesthesia was induced by intramuscular injection of ketamine hydrochloride (approximately 10 mg/kg) and after endotracheal intubation maintained by administration of a mixture of sevoflurane (2–8%), oxygen, and medical air. Head immobilization and safety monitoring procedures (body temperature, heart rate, blood pressure, fluid balance) were performed as described previously (Shou et al 2019).

The radioligand [^{11}C]VC-002 was prepared at the PET center at Karolinska University Hospital as previously described (Visser et al 1997, Schou et al 2019). In each PET measurement, a sterile physiological, phosphate-buffered (pH 7.4) saline (PBS) solution containing [^{11}C]VC-002, in a volume not exceeding 5mL, was injected as a bolus into a sural vein during 5 s. PET data acquisition started at time of the bolus injection.

PET measurements were conducted using the high-resolution research tomograph (HRRT) (Siemens Molecular Imaging). Radioactivity in lungs was measured continuously over 63 min using an imaging protocol described in detail previously (Schou et al 2019). In short, a transmission scan of 6 min using a single ^{137}Cs source was performed immediately before [^{11}C]VC-002 injection. Data were acquired continuously in list mode for 63 min after i.v. injection of [^{11}C]VC-002. Images were reconstructed for a series of time frames (9 × 10 s, 2 × 15 s, 3 × 20 s, 4 × 30 s, 4 × 1 min, 4 × 3 min, and 7 × 6 min).

Blood sampling for the measurement of radioactivity

Venous blood samples (1–3 mL) were obtained manually at 1, 2, 3, 5, 15, 30, 45 and 60 min for the measurement of radioactivity in whole blood and plasma using a well-counter. The procedure has previously been described in detail (Schou et al 2019).

Region of interest definition

Regions of interest (ROIs) were manually delineated for the lungs (pooled) and the arch of the thoracic aorta on the summation (0–60 min integral) and the early (0–2 min) PET images, respectively. The ROIs were applied to the series of PET images to generate time-activity curves (TACs).

Study in humans

Subjects and study design

The study was approved by the Regional Ethics Committee in Stockholm and the Radiation Protection Committee at the Karolinska University Hospital, Stockholm. Written informed consent was obtained from each subject.

Seven male subjects, 20–50 years of age, were recruited and studied at the PET Centre, Department of Clinical Neuroscience, Karolinska Institutet, Stockholm, Sweden. Subjects were healthy according to medical history, clinical examination, and routine laboratory blood and urine tests. No medications were allowed at time of the study.

The PET-measurements were carried out on a whole-body GE Discovery 710 PET/CT-system at the Department of Nuclear Medicine, Karolinska University Hospital, Solna. Each subject participated in two or three PET examinations that were performed on separate days.

In part 1, subjects H1-H3 first participated in a baseline (BL) measurement. A second PET measurement was performed 7–12 days later 2 hours after inhalation of a therapeutic dose of tiotropium (18 µg).

In part 2, each of four subjects H4-H7 participated in three PET measurements. The first PET (BL) was followed by two PET measurements, each one after pretreatment with tiotropium (18 µg). The pretreatment PET measurements started 30 min after inhalation of tiotropium in subjects H4-H5 and 2 hours after inhalation in subjects H6-H7 (for details see Supplement Fig. 2). In both study parts, adverse events were monitored on experimental days and up to one week after the last measurement via a follow-up telephone call.

Measurement of tiotropium plasma concentration

In part 1 (subjects H1-H3) the concentration of tiotropium in plasma was not measured. In part 2 (subjects H4-H7), 3 venous blood samples were obtained at start, middle time and end of the PET measurement, i.e. 30–90 or 120–180 min post inhalation of tiotropium. A standard LC-MS/MS analysis of tiotropium concentration in venous plasma was performed (Hohlfeld et al 2014). The lower limit of quantification (LLOQ) was 1.3 pM. The average concentration during PET acquisition was obtained by calculating the area under the plasma concentration curve and dividing it by the duration of PET.

PET/CT measurements

PET examinations, radiochemistry, blood sampling, image processing, and quantification were performed essentially as described in detail in our previous publication on the test-retest reliability of [^{11}C]VC-002 binding in the human lung (Cselényi et al 2020).

In short, at time of imaging examination each subject was positioned in the PET/CT system head-first, supine with the chest located within the 16 cm field of view. Initially, a low-dose CT was obtained for the chest. After i.v. injection of [^{11}C]VC-002, radioactivity was acquired in list mode for 63 min providing a reconstructed 4D PET image with 33 timeframes with equivalent frame timings as for the NHP study.

The PET image was evaluated and, if possible, corrected for inter-frame subject movements as described previously (Cselényi et al 2020). In short, the reconstructed 4D PET image was frame-by-frame realigned to have a consistent subject position throughout. In case of mismatch of the PET frame and the CT scan used for attenuation correction, the PET image was re-reconstructed to minimise this effect of a movement artifact, by ensuring the correct alignment of the attenuation map for each time frame. The final corrected image was quality checked for the presence of potential residual artifacts related to severe intraframe subject movement.

Blood sampling for measuring [^{11} C]VC-002 radioactivity concentration

Before PET an arterial cannula was inserted into one of the radial arteries. After injection of [^{11}C]VC-002, 3 arterial blood samples (2 ml each) were drawn manually at 10, 25, and 45 min for the purpose of determining the average plasma-to-whole-blood ratio.

Regions of interest delineation

ROIs for the lungs and the arch of the aorta were delineated automatically as described previously (Cselényi et al 2020). In short, the method relied on the co-registered CT images to identify voxels in the body with a density below water based on the CT Hounsfield unit value. The binary image of such voxels was then refined using the summation PET image and image processing morphological operations to arrive at identifying a ROI covering both lungs. Voxels falling within the volume of the arch of the aorta were identified based on the voxels' early time course of high radioactivity after iv. injection. In addition, the search was restricted to the mediastinal space, and distinguished between venous (e.g. vena cava) and arterial voxels based on the relative timing of peak radioactivity. Finally, the ROIs were applied to the series of PET images to obtain TACs for the whole lung (bilateral) and aorta, respectively.

Quantification of radioligand binding and receptor occupancy

Quantification of [^{11} C]VC-002 binding in lungs

The total plasma radioactivity concentration was used as the input function for quantification of binding as previously described (Schou et al 2019, Cselényi et al 2020). To derive this curve, the TAC for the aorta was multiplied with the average plasma-to-whole-blood radioactivity ratio calculated from the drawn blood samples as described above.

The parameter used to express [^{11}C]VC-002 binding was the total volume of distribution (V_T), which is an index of total binding in tissue, i.e. the sum of non-specific and receptor-specific binding. V_T is numerically equivalent to the tissue partition coefficient, i.e. the ratio of tissue to plasma concentration in case of proper steady state conditions.

The quantification was carried out for each volume element (voxel) using data-driven estimation of parametric images based on compartmental theory (DEPICT), as described previously (Gunn et al 2002, Cselényi et al 2020). The range of exponents, employed in the calculation of the table of kinetic basis

functions used by DEPICT, was between 0.0136 1/min and 0.6 1/min (as per Gunn et al 2002). The main output of DEPICT was voxel-wise parametric images of V_T in the lungs.

Quantification of receptor occupancy

Receptor occupancy calculation is straightforward when the availability of a reference region with negligible binding provides an estimate of non-specific binding and thus allows for differentiation between specific and non-specific binding in the target region. However, in pulmonary imaging there is no reference region and the specific binding component of a radioligand such as [^{11}C]VC-002 cannot be directly quantified (Cselényi et al 2020). The estimation of receptor occupancy following drug administration was instead estimated using the Lassen plot, an established indirect approach (Lassen et al 1995, Cunnigham et al 2010).

The indirect Lassen approach is based on the total binding (V_T) values and relies on the assumptions that: 1) various parts of the lungs have different levels of mAChR expression, and specific [^{11}C]VC-002 binding, while 2) the background of non-specific binding as well as drug exposure at the target is similar across the organ. Based on these assumptions, lung V_T data from baseline and pretreatment conditions were entered into a graphical evaluation (Lassen plot), which provided estimates of receptor occupancy as well as the level of non-specific (non-displaceable) binding, V_{ND} (Lassen et al 1995, Ichise et al 2002, Cunnigham et al 2010). For this purpose, the V_T parametric images were first downsampled to a lower resolution to reduce the voxel-wise, noise-related variance. Voxel-wise V_T data were then extracted for the Lassen plot analysis. A detailed description of the procedure is given in the supplement.

The presently obtained receptor occupancy values were compared to the previously reported test-retest study in humans (Cselényi et al 2020). For that purpose, the test-retest dataset was re-analysed using the same settings as in the present study, i.e. using only the first 63 min of the acquired data and the same DEPICT settings as specified above.

Assessment of the plasma exposure–occupancy relationship

The occupancy values obtained from the Lassen plot were entered into an analysis of the curvilinear relationship between drug plasma concentration and pulmonary receptor occupancy. In detail, a weighted non-linear least square curve fit was performed using the following equation:

$$Occ = Occ_{max} \times \frac{C_p}{C_p + K_i} \quad \text{Eq. 1}$$

where Occ is occupancy, Occ_{max} is the maximum level of occupancy achievable by tiotropium at the target binding sites detected by [^{11}C]VC-002, C_p is the average plasma tiotropium concentration during PET and K_i is the apparent inhibition constant, i.e. the plasma concentration when Occ equals half of Occ_{max}.

The model was fitted to the occupancy values estimated obtained from the Lassen plot analysis, yielding estimates of K_i. The maximal occupancy, Occ_{max}, was either fixed at 100% or, alternatively, estimated by the

fit. The R-squared values of the linear fit in the Lassen plot occupancy estimation were used as weighting factors when fitting the occupancy model, i.e. in effect giving more weight to occupancy values that were more certain. The model was fitted in separate analyses to NHP (i.v. administration-based) and human (inhalation based) data, respectively.

Statistics

Processing and computations were performed using the Matlab, version R 2014b (www.mathworks.com). The estimation of occupancy using weighted linear least squares provided statistical assessment of the goodness-of-fit, such as the coefficient of determination, R^2, the standard error and a 95% confidence interval for the coefficients. A simple t-test was separately performed on the inter-individual mean occupancy values for each group (pretreatment or test-retest) and species (NHP or human). Statistical assessment was performed on the results of the exposure–occupancy model fits: 1) to ascertain the goodness of fit (among others calculating the standard error and 95% confidence interval of fitted parameters), 2) to compare alternative models of the NHP data (by using an F-test, Akaike's information criterion values, AIC, and adjusted R-squared values), and 3) to compare i.v. administration based (NHP) and inhalation based (human) K_i estimates (by using two-tailed t-tests). In all analyses, the statistical significance (alpha level) was set at $p < 0.05$.

Results

Study in NHPs

Tiotropium plasma concentration

The measured average tiotropium plasma concentrations in NHP covered a wide interval, ranging from sub-therapeutic levels (~ 2 pM) to supra-therapeutic levels (~ 300 pM).

For NHP1, in the 2nd baseline plus pretreatment session (0.03 µg/kg tiotropium dose), only the first post-injection sample had a value above LLOQ. The concentration value used for further analysis was obtained after extrapolating the curve with the help of a reference plasma concentration curve, scaled to the measured peak value (see Supplemental Fig. S2).

PET measurements and [^{11} C]VC-002 binding in lungs

In all measurements the radiochemical purity of [^{11}C]VC-002 exceeded 99% at time of injection. In NHPs, the mean radioactivity injected was 154 MBq (SD ± 9 MBq, range 139–172 MBq, N = 16 measurements). The molar activity at time of injection was 689 GBq/µmol (SD ± 814 GBq/µmol, range 129–3195 GBq/µmol) corresponding to an injected mass of 0.25 µg (SD ± 18 µg, range 0.025–0.57 µg).

Visual inspection of the PET-images obtained after intravenous injection of [^{11}C]VC-002 showed that the radioactivity was distributed throughout the lungs (Fig. 1). Compared to the radioactivity concentration in

lungs, the radioactivity in heart tissue and liver was at a substantially higher level. After administration of tiotropium, there was an conspicuous reduction in radioactivity in lungs and heart, but not liver (Fig. 1).

The reduction in radioactivity after tiotropium was also evident when inspecting the TACs for the lungs (Fig. 2A). For plasma, there was no systematic difference when comparing pretreatment and baseline conditions (Fig. 2B). Accordingly, the plots visualising the ratio of lung tissue to plasma over time showed a marked effect of pretreatment with tiotropium (Fig. 2C).

Parametric images of V_T also demonstrated a reduction in total binding in lungs after pretreatment (Fig. 3A). The whole lung total binding of [^{11}C]VC-002 was reduced in a dose dependent manner up to 63% in NHP following pretreatment but was on average unchanged at test-retest conditions (Table 1).

Receptor occupancy in lung tissue

The occupancy at the [^{11}C]VC-002 binding sites induced by tiotropium was quantified using the Lassen plot (Fig. 3B). and varied between 11 and 78%. The values were overall significantly different from zero ($p = 0.008$, two-tailed t-test) (Fig. 4A, Table 1). Furthermore, the V_{ND} estimates obtained from the Lassen plots indicated that non-displaceable binding in lung tissue was on average 10% of the baseline total binding (Table 1). The analysis of the two test-retest datasets (NHP1 and NHP2) yielded a Lassen plot estimate of 0, i.e. no “occupancy”. These values were used for comparative purposes (Fig. 4A, Table 1).

Plasma exposure-receptor occupancy relationship

The occupancy values were plotted versus the plasma concentration for the six pretreatment measurements in NHP (Fig. 4B, 4C). The data could be described by a curvilinear relationship according to Eq. 1. K_i, the apparent inhibition constant, which corresponds to the plasma concentration when half of the drug-targeted binding sites are occupied was estimated. Fitting the model with an Occ_{max} parameter fixed at 100% yielded a K_i estimate of 84.3 pM (95% CI: 43.2–164.6 pM) (Fig. 4B). Alternatively, the non-fixed model fit yielded a K_i estimate of 29.1 pM (95% CI: 11.2–75.5 pM) and an Occ_{max} estimate of 79.6% (95% CI: 66.2–93.0%) (Fig. 4C). The non-fixed model fit provided a better description of plasma concentration–occupancy data both visually and according to statistical assessment with the one-tailed F-test (F-value 9.65, p-value: 0.036), or when comparing Akaike’s Information Criterion values (AIC: 36.5 for the first model vs. 31.2 for the second model) or the adjusted R-squared values of the fitted models (0.59 for the first model vs. 0.85 for the second model).

Study in humans

Subjects and data acquisition

Seven male subjects, mean age 34 years (range 23 to 49 years) participated in the study. In each subject, the PET examinations were carried out at least 2 days apart.

The baseline PET for subject H6 was not possible to evaluate due to severe movement artefacts throughout the experiment. These movement artifacts could not be corrected for by the frame-by-frame correction procedure described in the methods section. Dosing failed for subject H4 in the first pretreatment measurement. The inhaler was by mistake not loaded with tiotropium, thus, effectively resulting in a repeated baseline (retest) measurement. Furthermore, the plasma analysis was inconclusive in subject H5.

Tiotropium plasma concentration

The measured average tiotropium concentrations were in the range of 3.6–6.1 pM (4.4 ± 1.0 nM, N = 5) and were compared to a previously obtained reference curve showing the expected levels for a therapeutic dose (supplemental Fig. S2). The values obtained in the present study are almost 3-fold lower than the reference data.

PET measurements and [^{11} C]VC-002 binding in lungs

The radiochemical purity of [^{11}C]VC-002 exceeded 99% at time of injection in all measurements. The mean injected radioactivity was 220 MBq (SD ± 37 MBq, range 165–296 MBq, N = 18) and the molar activity was 398 GBq/μmol (SD ± 250 GBq/μmol, range 51–955 GBq/μmol). The corresponding mass of the radioligand injected was 0.34 μg (SD ± 0.34, range 0.08–1.24 μg).

As in NHP, the radioactivity was distributed throughout the lungs following intravenous injection of [^{11}C]VC-002 (Fig. 5) with high levels also in heart tissue and liver. The radioactivity in lungs and heart, but not liver, was reduced following tiotropium inhalation. This reduction could also be observed on the TACs for the lungs (Fig. 6A). The plasma TACs did not display an evident systematic difference between baseline and pretreatment measurements (Fig. 6B). Accordingly, the plots showing the ratio of radioactivity in lungs to plasma over time indicated a reduction in [^{11}C]VC-002 binding after tiotropium inhalation (Fig. 6C).

Parametric images of V_T also indicated reduced [^{11}C]VC-002 binding in lungs after tiotropium inhalation (demonstrated in Fig. 7A). The average reduction in total binding of [^{11}C]VC-002 in lung tissue was close to 20% (maximum 27%) in humans following pretreatment (Table 1). By comparison, on average there was no change in whole-lung V_T at test-retest when analysing the 8 subjects from our previous publication (Cselényi et al 2020).

Receptor occupancy in lung tissue

The Lassen plot was used to estimate mAChR occupancy in lungs as demonstrated for a single subject in Fig. 7B. Following tiotropium inhalation, the occupancy estimates in the 10 measurements varied from 6 to 65% (Fig. 8A, Table 1). They were overall significantly different from zero ($p = 0.0003$, two-tailed t-test). The level of non-displaceable binding (V_{ND}) was about 20% of total binding in lung tissue at baseline (Table 1). Lassen-plot based estimates in the test-retest datasets were below 6% (Table 1).

Plasma exposure–occupancy relationship

The tiotropium plasma concentration–occupancy data in human fell in a relatively narrow plasma exposure range with a large variation in occupancy values (Fig. 8B). As such, only the exposure–occupancy model with a fixed Occ_{max} of 100% could be readily applied, which yielded a K_i estimate of 6.8 pM (95% CI: 2.0–22.7 pM) (Fig. 8B). Two-tailed t-tests comparing the human (inhalation-based) K_i estimate to those obtained in NHP (following i.v. administration, Fig. 4B, C) indicated a significant difference between the two administration routes and species (p-values below 0.0003).

Discussion

In a translational setting we demonstrated an evident effect of the long-acting muscarinic antagonist tiotropium on [^{11}C]VC-002 binding to muscarinic receptors in lungs in both NHPs and humans. A wide dose range of tiotropium was examined in NHPs. The binding was reduced in a saturable dose-dependent fashion and at the largest dose the total binding (V_T) in the whole lung was reduced by about two thirds (Table 1). This result suggests that a major proportion of the total [^{11}C]VC-002 binding in lung represents specific binding to mAchR, whereas a minor proportion represents a background of free and non-specific [^{11}C]VC-002 binding.

Furthermore, the Lassen plot analysis provided direct estimates of the reduction of specific binding, i.e. the mAchR occupancy. The occupancy reached 80% for the highest tiotropium dose (1.0 ug/kg). Interestingly, the saturation curve analysis of the exposure – occupancy data in NHPs indicated that the projected maximum occupancy possibly achievable by tiotropium at the binding sites recognized by [^{11}C]VC-002 was less than 100% (Occ_{max}=80%). The composition of the remaining, non-displaceable portion is however not clear. Besides representing free and non-specific binding it has to be considered that both [^{11}C]VC-002 and tiotropium are non-selective compounds with high affinity for M1-M3 muscarinic subtypes (Visser et al, 1997; Haddad et al 1994). However, both compounds have different affinity profiles across the M1-M3 receptors, thus, tiotropium may not fully block all [^{11}C]VC-002 binding and by that contribute to the estimated non-specific compartment.

In humans, high doses of tiotropium could not be examined for safety reasons. In the present study, only a single, therapeutic dose of 18 µg was evaluated and the reduction of total [^{11}C]VC-002 binding was small when compared to the effect of high dose i.v. administration of tiotropium in NHP. Only moderate lung occupancy was detected with estimated values mostly below 50% (range 6–65%). Importantly, a potential limitation is that the study was performed in a group of healthy subjects, who had no previous experience with inhalation apart from a short training session. As such, inhalation of tiotropium may have been suboptimal, which could explain the approximately 3-fold lower plasma exposure than expected as defined for a therapeutic dose (see supplemental Fig. S1). Thus, the moderate mAChR occupancy may have been due to tiotropium underexposure.

There was a significant difference between the estimated *in vivo* affinity in the two species with roughly one order of magnitude larger NHP K_i values (29.1 or 84.3 pM depending on model) than the human K_i value (6.8 pM). Species differences may play a role here, though the muscarinic receptor protein sequences

are highly homogeneous between NHPs and humans. In detail, there are only 3 (out of 466) amino-acid differences for the M2 receptor and 9 (out of 590) differences for the M3 receptor, all only in non-ligand-binding regions of the proteins (National Center for Biotechnology Information (NCBI) protein database, Home - Protein - NCBI (nih.gov)). A more likely explanation is thus provided by the differences in the route of administration, i.e. inhalation in NHP vs. intravenous infusion in human. Importantly, prior work, executed in NHP using ipratropium has demonstrated a similar difference in apparent potency between the two administration routes only in lung but not in other mAchR-rich organs (Shou et al 2019). This difference demonstrates the *targeting effect* of inhalation, which translates to the clinical benefit of achieving therapeutic drug effect in lungs while minimizing side effects due to muscarinic blockade in other organs such as the heart.

A further aspect of characterizing drug target engagement is the time course of receptor occupancy following inhalation. Detailed evaluation of the time course was beyond the scope of the present work. Anyhow, in a preliminary attempt we examined the level of occupancy in a one-hour-long acquisition window starting at 30 min and 2 hours post inhalation, respectively. The results indicated detectable lung occupancy of similar magnitude at both time intervals. Ideally, PET experiments with a displacement paradigm, i.e. drug inhalation during an ongoing [^{11}C]VC-002 PET acquisition, could be used to assess the early and detailed time course of lung occupancy. The off-rate of specific binding of [^{11}C]VC-002 is sufficiently high (above 0.1 1/min) to perform displacement experiments (Cselényi et al 2020).

Subject movement during PET acquisition poses a challenge to evaluating radioligand binding and thus drug effect in lungs. In the present work, a previously described frame-by-frame correction approach was used to address this issue (Cselényi et al 2020). While yielding acceptable results in most cases, the method has a limitation when subjects have substantial intra-frame movement which cannot be corrected using this scheme, such as it happened in one case in the current study (baseline PET for subject H6).

Another limitation was that fractional air content inhomogeneities were not corrected for in the results, chiefly because NHP had no CT images necessary for the correction. Theoretically, air-content related inhomogeneities may lead to violation of the underlying assumptions of the Lassen plot, such as an even level of non-displaceable binding across the organ. However, in the present study the assumption appeared to be supported by the predominantly linear distribution of the Lassen plot across scatter points. Nonetheless, incorporating air-content correction could prove to be beneficial in occupancy studies in patients who have more extreme lung compositional inhomogeneities such as fibrosis and emphysema.

New targets for respiratory drug development have been identified in current research on the pathophysiology of chronic pulmonary disorders. The list of emerging targets include integrin, lysophosphatidic acid receptor, FAPI, adrenomedullin receptors and, CCR2, among others. Such drug discovery and development projects invigorate application of pulmonary imaging using PET (Martinez et al 2018, Niemeijer et al 2018, Maher et al 2020, Bergman et al 2021, Brody et al 2021). Worth noting is that besides the present study, several recent studies have aimed to develop and apply quantitative techniques (Gallezot et al 2017, Harris et al 2007, Lukey et al 2020) for PET studies on the pathophysiology of pulmonary disorders as well as in development of novel treatments.

Conclusions

In conclusion, the present study demonstrated that [^{11}C]VC-002 binds specifically to mAChRs in the lungs such that it allows for the detection and quantification of receptor occupancy following administration of intravenously injected as well as inhaled muscarinic antagonist drugs. The methodology has potential for dose finding and comparison of drug formulations in future applied studies.

Abbreviations

AIC: Akaike's information criterion; BL: baseline; CNS: central nervous system; COPD: chronic obstructive pulmonary disorder; CT: computerised tomography; DEPICT: Data-driven Estimation of Parametric Images based on Compartmental Theory; HPLC: high-performance liquid chromatography; HRRT: high-resolution research tomograph; I.V.: intravenous; LAMA: long-acting mAChR antagonist; LLOQ: lower limit of quantification; mAChR: muscarinic acetylcholine receptor; NCBI: National Center for Biotechnology Information; NHP: non-human primate; Occ: occupancy; PBS: phosphate-buffered saline; PET: positron emission tomography; RO: receptor occupancy; ROI: region of interest; SD: standard deviation; TAC: time-(radio)activity curve; [^{11}C]VC-002: N-[11C]-methyl-piperidin-4-yl-2-cyclohexyl-2- hydroxy-2-phenylacetate; V_T: total volume of distribution

Declarations

Ethics approval and consent to participate: All procedures performed in studies involving human participants were in accordance with the ethical standards of the institutional and/or national research committee and with the 1964 Helsinki declaration and its later amendments or comparable ethical standards. Specifically, the study was approved by the Regional Ethics Committee in Stockholm and the Radiation Protection Committee at the Karolinska University Hospital, Stockholm. Written informed consent was obtained from each subject.

Consent for publication: Not applicable.

Availability of data and materials: The datasets used and/or analysed during the current study are available from the corresponding author on reasonable request.

Competing interests: ZC, AJ, PJ, MS, KG, PE, CK, BL, UGE are employees of AstraZeneca and may own stock or stock options. LF owns stocks in AstraZeneca. The other authors have no disclosures to report.

Funding: This study was funded by AstraZeneca.

Authors' contributions: ZC, AJ, CK, PE, PJ, MS, CH, KG, UGE and LF contributed to conception of the work and all authors contributed to the design of the study. PS, AV, PJ, MS, AVR, MMM, MB, JS, PG, BL contributed to study conduct and data acquisition. ZC performed method development and image analysis. All authors were involved in results interpretation. All authors reviewed and approved the final manuscript.

Acknowledgements: We thank all participants involved in this project for their cooperation. We thank the members of the PET Centre, Karolinska Institutet for performance of the PET study in non-human primates and for the study conduct in humans. We thank Per Grybäck, Jonathan Siikanen and other members of the Nuclear Medicine Department, Karolinska University Hospital for the study set-up, imaging data collection and primary workup.

References

1. Melani AS. Long-acting muscarinic antagonists. Expert Rev Clin Pharmacol. 2015;8(4):479-501. https://doi.org/10.1586/17512433.2015.1058154
2. Maia IS, Pincelli MP, Leite VF, Amadera J, Buehler AM. Long-acting muscarinic antagonists vs. long-acting β 2 agonists in COPD exacerbations: a systematic review and meta-analysis. J Bras Pneumol. 2017;43(4):302-12. https://doi.org/10.1590/S1806-37562016000000287
3. Matera MG, Page CP, Calzetta L, Rogliani P, Cazzola M. Pharmacology and Therapeutics of Bronchodilators Revisited. Pharmacol Rev. 2020;72(1):218-52. https://doi.org/10.1124/pr.119.018150
4. Mastrodicasa MA, Droege CA, Mulhall AM, Ernst NE, Panos RJ, Zafar MA. Long acting muscarinic antagonists for the treatment of chronic obstructive pulmonary disease: a review of current and developing drugs. Expert Opin Investig Drugs. 2017;26(2):161-74. https://doi.org/10.1080/13543784.2017.1276167
5. Lal C, Khan A. Emerging Treatments for COPD: Evidence to Date on Revefenacin. COPD. 2020;17(1):112-119. https://doi.org/10.1080/15412555.2019.1702010
6. Bäckman P, Adelmann H, Petersson G, Jones CB. Advances in inhaled technologies: understanding the therapeutic challenge, predicting clinical performance, and designing the optimal inhaled product. Clin Pharmacol Ther. 2014;95(5):509-20. https://doi.org/10.1038/clpt.2014.27
7. Farde L, Wiesel FA, Halldin C, Sedvall G. Central D2-dopamine receptor occupancy in schizophrenic patients treated with antipsychotic drugs. Arch Gen Psychiatry. 1988;45(1):71-6. https://doi.org/10.1001/archpsyc.1988.01800250087012
8. Waarde Av. Measuring receptor occupancy with PET. Curr Pharm Des. 2000;6(16):1593-610. https://doi.org/10.2174/1381612003398951
9. Lee CM, Farde L. Using positron emission tomography to facilitate CNS drug development. Trends Pharmacol Sci. 2006;27(6):310-6. https://doi.org/10.1016/j.tips.2006.04.004
10. Varnäs K, Nyberg S, Karlsson P, Pierson ME, Kågedal M, Cselényi Z, McCarthy D, Xiao A, Zhang M, Halldin C, Farde L. Dose-dependent binding of AZD3783 to brain 5-HT1B receptors in non-human primates and human subjects: a positron emission tomography study with [11C]AZ10419369. Psychopharmacology (Berl). 2011;213(2-3):533-45. https://doi.org/10.1007/s00213-011-2165-z
11. Nord M, Nyberg S, Brogren J, Jucaite A, Halldin C, Farde L. Comparison of D□ dopamine receptor occupancy after oral administration of quetiapine fumarate immediate-release and extended-release formulations in healthy subjects. Int J Neuropsychopharmacol. 2011;14(10):1357-66. https://doi.org/10.1017/S1461145711000514

12. Jucaite A, Cselényi Z, Lappalainen J, McCarthy DJ, Lee CM, Nyberg S, Varnäs K, Stenkrona P, Halldin C, Cross A, Farde L. $GABA_A$ receptor occupancy by subtype selective $GABA_{A\alpha 2,3}$ modulators: PET studies in humans. Psychopharmacology (Berl). 2017;234(4):707-716. https://doi.org/10.1007/s00213-016-4506-4
13. Schou M, Ewing P, Cselenyi Z, Fridén M, Takano A, Halldin C, Farde L. Pulmonary PET imaging confirms preferential lung target occupancy of an inhaled bronchodilator. EJNMMI Res. 2019;9(1):9. https://doi.org/10.1186/s13550-019-0479-8
14. Cselényi Z, Jucaite A, Kristensson C, Stenkrona P, Ewing P, Varrone A, Johnström P, Schou M, Vazquez-Romero A, Moein MM, Bolin M, Siikanen J, Grybäck P, Larsson B, Halldin C, Grime K, Eriksson UG, Farde L. Quantification and reliability of [^{11}C]VC - 002 binding to muscarinic acetylcholine receptors in the human lung - a test-retest PET study in control subjects. EJNMMI Res. 2020;10(1):59. https://doi.org/10.1186/s13550-020-00634-0
15. Visser TJ, van Waarde A, Jansen TJ, Visser GM, van der Mark TW, Kraan J, Ensing K, Vaalburg W. Stereoselective synthesis and biodistribution of potent [11C]-labeled antagonists for positron emission tomography imaging of muscarinic receptors in the airways. J Med Chem. 19973;40(1):117-24. https://doi.org/10.1021/jm960374w
16. Hohlfeld JM, Sharma A, van Noord JA, Cornelissen PJG, Derom E, Towse L, Peterkin V and Disse B. Pharmacokinetics and Pharmacodynamics of Tiotropium Solution and Tiotropium Powder in Chronic Obstructive Pulmonary Disease. J Clin Pharm. 2014; 54(4): 405–414. https://doi.org/10.1002/jcph.215
17. Gunn RN, Gunn SR, Turkheimer FE, Aston JA, Cunningham VJ. Positron emission tomography compartmental models: a basis pursuit strategy for kinetic modeling. J Cereb Blood Flow Metab. 2002 Dec;22(12):1425-39. https://doi.org/10.1097/01.wcb.0000045042.03034.42
18. Lassen NA, Bartenstein PA, Lammertsma AA, Prevett MC, Turton DR, Luthra SK, Osman S, Bloomfield PM, Jones T, Patsalos PN, et al. Benzodiazepine receptor quantification in vivo in humans using [11C]flumazenil and PET: application of the steady-state principle. J Cereb Blood Flow Metab. 1995;15(1):152-65. https://doi.org/10.1038/jcbfm.1995.17
19. Cunningham VJ, Rabiner EA, Slifstein M, Laruelle M, Gunn RN. Measuring drug occupancy in the absence of a reference region: the Lassen plot re-visited. J Cereb Blood Flow Metab. 2010;30(1):46-50. https://doi.org/10.1038/jcbfm.2009.190.
20. Ichise M, Toyama H, Innis RB, Carson RE. Strategies to improve neuroreceptor parameter estimation by linear regression analysis. J Cereb Blood Flow Metab. 2002;22(10):1271-81. https://doi.org/10.1097/01.WCB.0000038000.34930.4E
21. Akaike H. A new look at the statistical model identification. IEEE Transactions on Automatic Control. IEEE, 1974, p. 716-723.
22. Haddad EB, Mak JC, Barnes PJ. Characterization of [3H]Ba 679 BR, a slowly dissociating muscarinic antagonist, in human lung: radioligand binding and autoradiographic mapping. Mol Pharmacol. 1994;45(5):899-907.

23. NCBI protein database: https://www.ncbi.nlm.nih.gov/protein Human M2 receptor sequence: https://www.ncbi.nlm.nih.gov/protein/NP_001365901.1 The NHP (Macaca mulatta) M2R sequence: https://www.ncbi.nlm.nih.gov/protein/XP_014990471.1 Human M3R: https://www.ncbi.nlm.nih.gov/protein/NP_001362913.1 NHP M3R: https://www.ncbi.nlm.nih.gov/protein/NP_001244669.1
24. Bergström M, Nordberg A, Lunell E, Antoni G, Långström B. Regional deposition of inhaled 11C-nicotine vapor in the human airway as visualized by positron emission tomography. Clin Pharmacol Ther. 1995;57(3):309-17. https://doi.org/10.1016/0009-9236(95)90156-6
25. Berridge MS, Lee Z, Heald DL. Regional distribution and kinetics of inhaled pharmaceuticals. Curr Pharm Des. 2000;6(16):1631-51. https://doi.org/10.2174/1381612003398852
26. Alonso Martinez LM, Harel F, Létourneau M, Finnerty V, Fournier A, Dupuis J, DaSilva JN. SPECT and PET imaging of adrenomedullin receptors: a promising strategy for studying pulmonary vascular diseases. Am J Nucl Med Mol Imaging. 2019;9(5):203-15.
27. Gallezot JD, Nabulsi NB, Holden D, Lin SF, Labaree D, Ropchan J, Najafzadeh S, Donnelly DJ, Cao K, Bonacorsi S, Seiders J, Roppe J, Hayes W, Huang Y, Du S, Carson RE. Evaluation of the Lysophosphatidic Acid Receptor Type 1 Radioligand ^{11}C-BMT-136088 for Lung Imaging in Rhesus Monkeys. J Nucl Med. 2018;59(2):327-33. https://doi.org/10.2967/jnumed.117.195073
28. Maher TM, Simpson JK, Porter JC, Wilson FJ, Chan R, Eames R, Cui Y, Siederer S, Parry S, Kenny J, Slack RJ, Sahota J, Paul L, Saunders P, Molyneaux PL, Lukey PT, Rizzo G, Searle GE, Marshall RP, Saleem A, Kang'ombe AR, Fairman D, Fahy WA, Vahdati-Bolouri M. A positron emission tomography imaging study to confirm target engagement in the lungs of patients with idiopathic pulmonary fibrosis following a single dose of a novel inhaled αvβ6 integrin inhibitor. Respir Res. 2020;21(1):75. https://doi.org/10.1186/s12931-020-01339-7
29. Niemeijer AN, Leung D, Huisman MC, Bahce I, Hoekstra OS, van Dongen GAMS, Boellaard R, Du S, Hayes W, Smith R, Windhorst AD, Hendrikse NH, Poot A, Vugts DJ, Thunnissen E, Morin P, Lipovsek D, Donnelly DJ, Bonacorsi SJ, Velasquez LM, de Gruijl TD, Smit EF, de Langen AJ. Whole body PD-1 and PD-L1 positron emission tomography in patients with non-small-cell lung cancer. Nat Commun. 2018;9(1):4664. https://doi.org/10.1038/s41467-018-07131-y
30. Bergmann C, Distler JHW, Treutlein C, Tascilar K, Müller A-T, Atzinger A, Matei A-I, Knitza J, Györfi A-H, Lück A, Dees C, Soare A, Ramming A, Schönau V, Distler O, Prante O, Ritt P, Theresa Ida Götz T I, Köhner M, Cordes M, Bäuerle T, Kuwert T, Schett G, Schmidkon C.68Ga-FAPI-04 PET-CT for molecular assessment of fibroblast activation and risk evaluation in systemic sclerosis-associated interstitial lung disease: a single-centre, pilot study. The Lancet Rheumatol. 2021; 3(3), p. e185-e19. https://doi.org/10.1016/S2665-9913(20)30421-5
31. Brody SL, Gunsten SP, Luehmann HP, Sultan DH, Hoelscher M, Heo GS, Pan J, Koenitzer JR, Lee EC, Huang T, Mpoy C, Guo S, Laforest R, Salter A, Russell TD, Shifren A, Combadiere C, Lavine KJ, Kreisel D, Humphreys BD, Rogers BE, Gierada DS, Byers DE, Gropler RJ, Chen DL, Atkinson JJ, Liu Y. Chemokine Receptor 2-targeted Molecular Imaging in Pulmonary Fibrosis. A Clinical Trial. Am J Respir Crit Care Med. 2021;203(1):78-89. https://doi.org/10.1164/rccm.202004-1132OC

32. Lukey PT, Coello C, Gunn R, Parker C, Wilson FJ, Saleem A, Garman N, Costa M, Kendrick S, Onega M, Kang'ombe AR, Listanco A, Davies J, Ramada-Magalhaes J, Moz S, Fahy WA, Maher TM, Jenkins G, Passchier J, Marshall RP. Clinical quantification of the integrin αvβ6 by [^{18}F]FB-A20FMDV2 positron emission tomography in healthy and fibrotic human lung (PETAL Study). Eur J Nucl Med Mol Imaging. 2020r;47(4):967-79. https://doiu.org/10.1007/s00259-019-04586-z
33. Harris RS, Schuster DP. Visualizing lung function with positron emission tomography. J Appl Physiol (1985). 2007 Jan;102(1):448-58. https://doi.org/10.1152/japplphysiol.00763.2006

Tables

Table 1. [^{11}C]VC-002 binding and receptor occupancy estimates

Species	Experiment	V_T, baseline Mean±SD (N)	V_T, follow-up Mean±SD (N)	V_T reduction (%) Mean (range)	Occupancy (%) Mean (range)	Occupancy (%) Median	V_{ND} Median
NHP	**Tiotropium**	1.6±0.6 (6)	1.1±0.6 (6)	36.4 (-0.4 – 62.7)	48.5 (11.1 – 77.9)	52.5	0.12
Human	**Tiotropium**	1.9±0.5 (6)	1.5±0.4 (10)	17.3 (2.3 – 26.7)	33.3 (6.4 – 65.0)	33.8	0.41
NHP	**Test-retest**	1.8±0.7 (2)	1.7±0.4 (2)	1.0 (-10.8 – 12.8)	0.0 (0.0 – 0.0)	0	0
Human	**Test-retest**	1.7±0.4 (6)	1.7±0.5 (6)	-5.4 (-28.1 – 3.6)	2.0 (0.0 – 5.4)	1.7	0

Summary statistics of [^{11}C]VC-002 binding and estimated receptor occupancy in lungs following tiotropium administration and test-retest experiments in non-human primates and humans. Binding was estimated using data-driven estimation of parametric images based on compartmental theory (DEPICT), occupancy was calculated using Lassen plot.

Figures

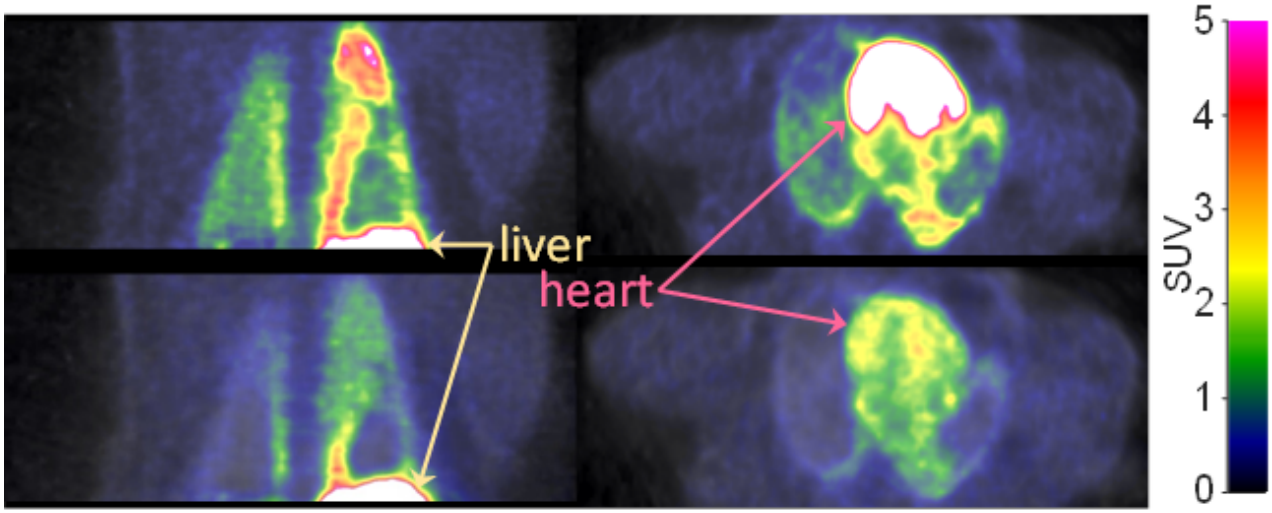

Figure 1

Positron emission tomography (PET) radioactivity images of [^{11}C]VC-002 in the non-human primate lungs

Images show frontal (left column) and horizontal (right column) slices through lungs. Data at baseline (upper row) and 20 min after the end of a 10-min intravenous infusion (lower row) of 1 µg/kg tiotropium are illustrated (individual subject NHP3).

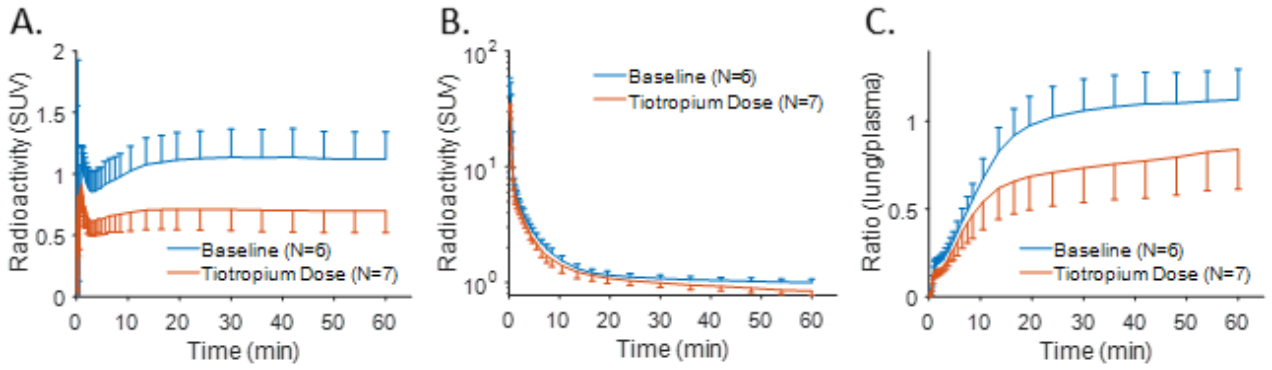

Figure 2

Regional curves for [^{11}C]VC-002 in non-human primate

Time-radioactivity curves for [^{11}C]VC-002 in lung (tissue-only) (**A**), plasma (**B**), and lung-to-plasma ratio (**C**). Curves show inter-individual mean with error bars indicating standard deviation.

Figure 3

Sample results of quantification of [^{11}C]VC-002 binding and occupancy in lung in non-human primate

Parametric images (**A**) of distribution volume V_T of [^{11}C]VC-002 in lung at baseline (upper row of images) and after tiotropium administration (lower row of images) (individual subject NHP3). Lassen plot data (NHP3) and linear fit used to obtain estimate of muscarinic receptor occupancy in lung (**B**). Straight line indicates linear fit with the x-axis intercept providing the V_{ND} and the slope providing the occupancy estimates, respectively.

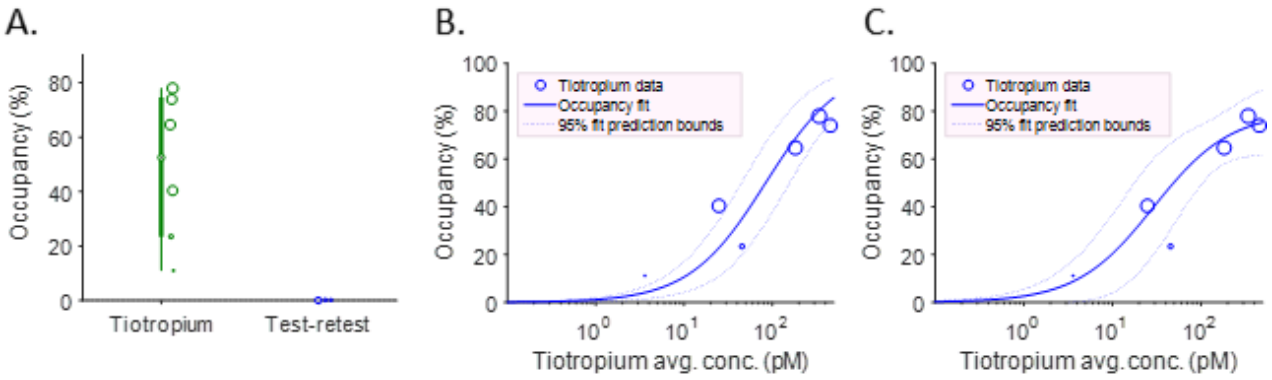

Figure 4

Estimated receptor occupancy and plasma exposure – occupancy relationship in non-human primates

Individual estimates and box plots of estimated receptor occupancy in lungs following tiotropium administration or under test-retest conditions (**A**). The boxplots indicate the median (black dots), inter-quartile range (thick vertical lines), and the minimum-maximum range (thin vertical lines). The size (area) of the individual circular markers, showing individual occupancy estimates, are proportional to the R^2 value of the linear fit used to obtain the occupancy , V_{ND} estimates. Model fit of the plasma exposure – receptor occupancy relationship for tiotropium providing estimate of apparent inhibition constant (K_i) with either fixed maximum occupancy (Occ_{max}) of 100% (**B**) or fitted Occ_{max} (**C**). Circular markers indicate tiotropium scatter point data (average plasma concentration during PET and lung muscarinic occupancy). For the fixed Occ_{max} model (**B**) the estimated K_i was 84.3 pM (95% CI: 43.2 – 164.6 pM), the adjusted R^2 value was 0.59, Akaike's Information Criterion (AIC) was 36.5. For the model with fitted Occ_{max} parameter (**C**) the estimated K_i was 29.1 pM (95% CI: 11.2 – 75.5 pM), the estimated Occ_{max} was 79.6% (95% CI: 66.2 –

93.0%), the adjusted R^2 value was 0.85 and AIC was 31.2. The one-tailed F-test comparing the two models had an F-value of 9.65 and a p-value of 0.036.

Figure 5

Positron emission tomography (PET) radioactivity images of [^{11}C]VC-002 in the human lungs

Images show frontal (left column) and horizontal (right column) slices through lungs. Data at baseline (upper row) and 20 min after the end of a 10-min intravenous infusion (lower row) of 1 µg/kg tiotropium are illustrated (individual subject S1).

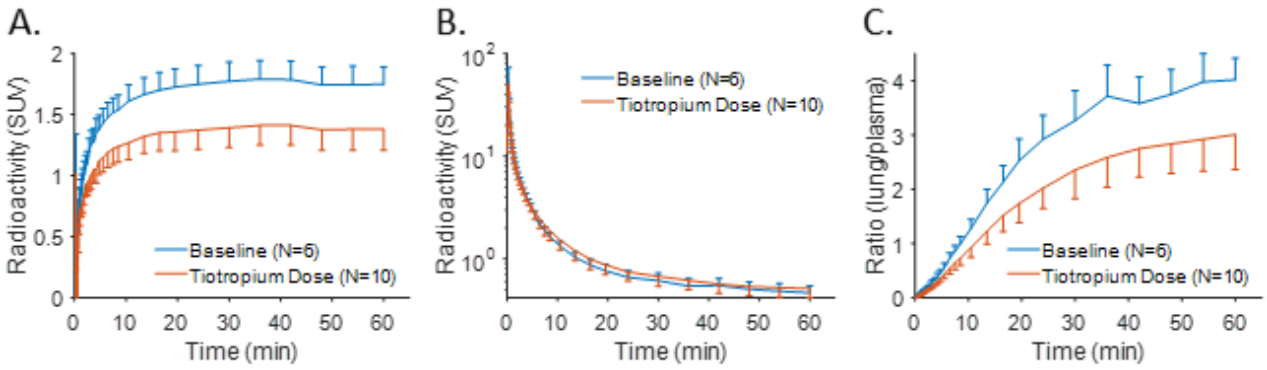

Figure 6

Regional curves for [^{11}C]VC-002 in human

Time-radioactivity curves for [^{11}C]VC-002 in lung (tissue-only) (**A**), plasma (**B**), and lung-to-plasma ratio (**C**). Curves show inter-individual mean with error bars indicating standard deviation.

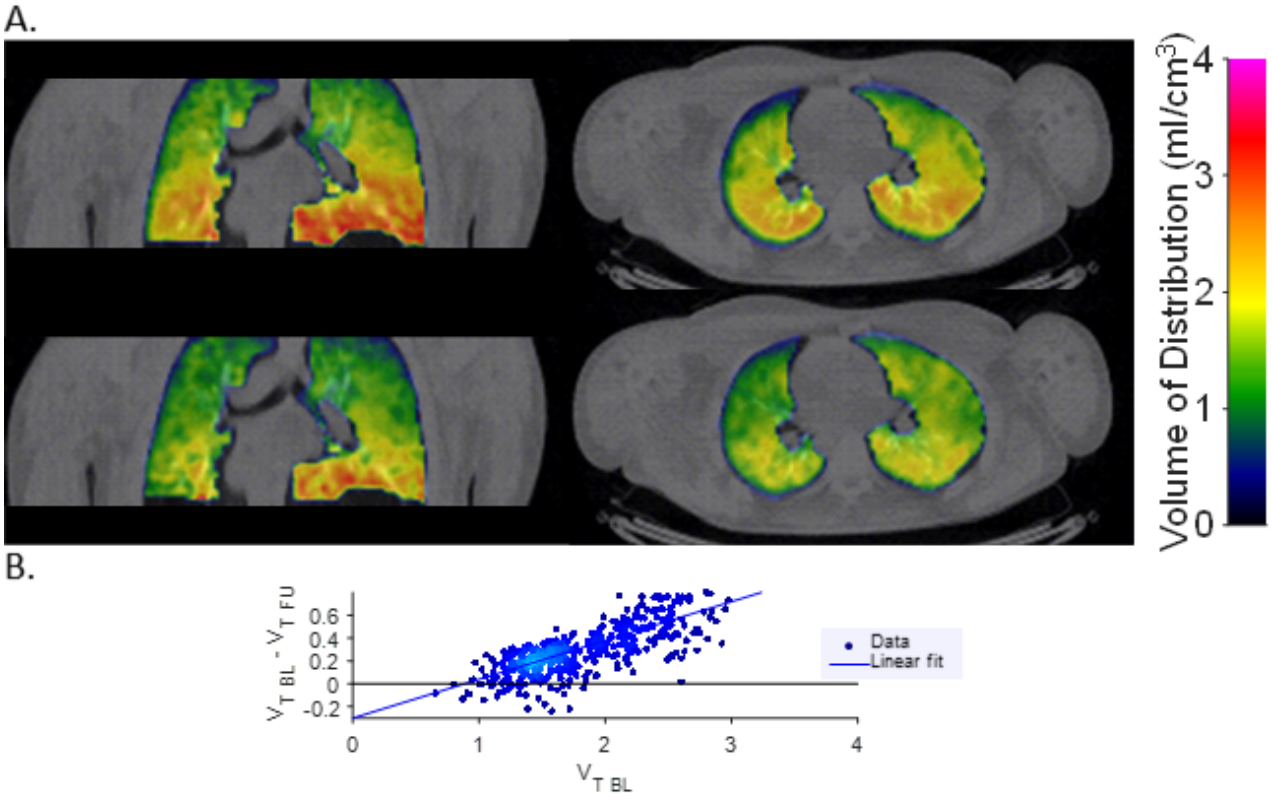

Figure 7

Sample results of quantification of [^{11}C]VC-002 binding and occupancy in lung in human

Parametric images (**A**) of distribution volume V_T of [^{11}C]VC-002 in lung at baseline (upper row of images) and after tiotropium administration (lower row of images) (individual subject S1). Lassen plot data (S1) and linear fit used to obtain estimate of muscarinic receptor occupancy in lung (**B**). Straight line indicates linear fit with the x-axis intercept providing the V_{ND} and the slope providing the occupancy estimates, respectively.

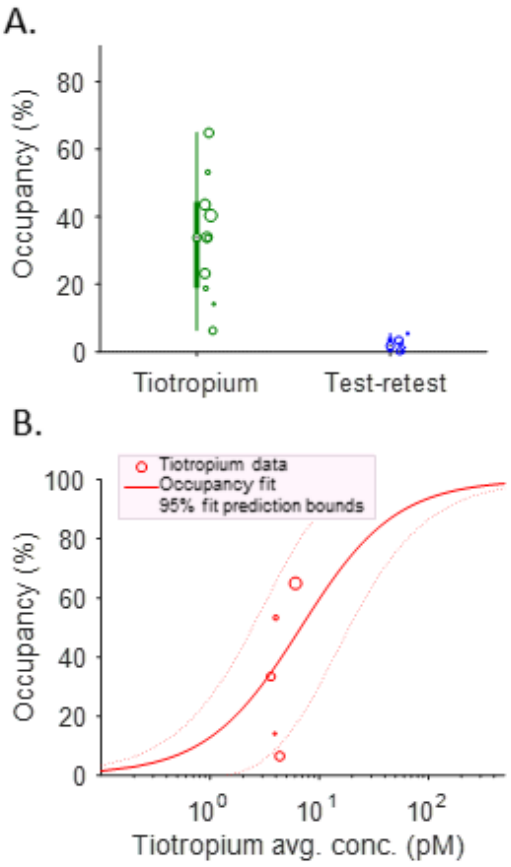

Figure 8

Estimated receptor occupancy and plasma exposure – occupancy relationship in human

Individual estimates and box plots of estimated receptor occupancy in lungs following tiotropium administration or under test-retest conditions (**A**). The boxplots indicate the median (black dots), inter-quartile range (thick vertical lines), and the minimum-maximum range (thin vertical lines). The size (area) of the individual circular markers, showing individual occupancy estimates, are proportional to the R^2 value of the linear fit used to obtain the occupancy, V_{ND} estimates. Model fit of the plasma exposure–receptor occupancy relationship for tiotropium providing estimate of apparent inhibition constant (K_i) with fixed maximum occupancy (Occ_{max}) of 100% (**B**). Circular markers indicate tiotropium scatter point data (average plasma concentration during PET and lung muscarinic occupancy). The estimated K_i was 6.8 pM (95% CI: 2.0 – 22.7 pM). Two-tailed t-tests comparing human, inhalation-based K_i to non-human primate (NHP), intravenous-administration-based K_i (see Fig. 4. B, C) had p-values <0.0003.

Supplementary Files

This is a list of supplementary files associated with this preprint. Click to download.

- supplementaldocument.docx